12th INTERNATIONAL SCIENTIFIC CONFERENCE ON DEFENSIVE TECHNOLOGIES
OTEH 2026
Serbia, Tara, 21 - 24 October 2026

SYSTEMATIC MODELING AND EXPERIMENTAL EVALUATION OF BLDC MOTOR-PROPELLER SYSTEMS IN MULTICOPTERS

ALJOŠA LJUBOJA
Military Technical Institute, Belgrade, aljosabiljana@gmail.com

MILENKO TRIFKOVIĆ
Military Technical Institute, Belgrade, milenkot@gmail.com

BRANISLAV OSTOJIĆ
Military Technical Institute, Belgrade, branislavostojic1994@gmail.com

TONI IVANOV
University of Belgrade, Faculty of Mechanical Engineering, Belgrade, tivanov@mas.bg.ac.rs

Abstract: *This paper presents a systematic methodology for assessing the performance of a multicopter propulsion system, focusing on the propeller, brushless direct current (BLDC) motor, electronic speed controller (ESC), and battery system. Addressing the challenge that current literature and datasheets on UAV performances especially concerning electric motors and propellers are usually scattered and poor. This research provides specific motor characteristics that are often difficult to find. By utilizing manufacturer technical specifications, mathematical models are used to evaluate critical metrics, including hover endurance, motor–ESC efficiency across the throttle range, payload capacity and tilt limits, and the optimization of speed and range in forward flight. Central to this research is the comprehensive experimental validation conducted using a motor thrust stand. Detailed experimental measurements of static thrust, torque, propeller RPM, and electricity consumption were performed to validate the numerical models. The results demonstrate a correlation between theoretical predictions and experimental data, confirming that the proposed methodology allows for reliable estimation of flight performance. This integrated approach provides a robust framework for engineers to effectively optimize component selection and accurately predict multicopter behavior.*

Keywords: *Multicopter, Propulsion System, BLDC Motor, Experimental validation.*

1. INTRODUCTION

The quadcopter is the most common multicopter unmanned-aerial-vehicle configuration. Vertical take-off and landing, hovering, low mechanical complexity and precise positioning support reconnaissance, surveillance, relay, logistics and specialized payload missions. In military applications, low observability, short preparation time, and the ability to operate outside the operator's direct line of sight are particularly important [1-3]. At the same time, low available battery energy and limited payload nevertheless remain primary constraints.

Performance depends on matching the propeller, brushless direct-current (BLDC) motor, electronic speed controller (ESC) and battery. Manufacturers do not publish a uniform data set: motor KV, current and resistance may be available, whereas a propeller is often described only by diameter, pitch and blade count. Static thrust and torque coefficients are consequently uncertain, especially at low Reynolds number, while forward flight additionally changes loading through advance ratio and disk incidence [4]. Low-order component models are useful in preliminary design because they connect a small parameter set to hover, endurance and mission estimates [5-7]. For forward flight and maneuvering conditions, where rotors operate under non-uniform and oblique inflow, propeller maps or suitable aerodynamic models are required [8-11]. A calculation based on a zero-advance ratio static test must therefore be reported as a conditional engineering screen rather than as measured flight performance.

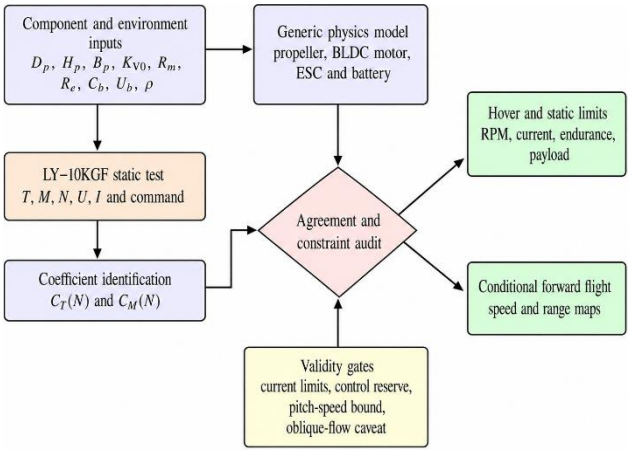


Figure 1. Workflow from confirmed hardware and LY-10KGF data to calibrated coefficients, constraint checks and conditional vehicle-level analysis

The objective is to determine operating points relevant to

Corresponding author: A. Ljuboja;
E-mail: aljosabiljana@gmail.com

DOI: 10.5937/OTEH26003L

hover and high loading, identify ESC and motor constraints, estimate payload, tilt, speed and range, and quantify agreement with a stationary thrust stand experiment. Four experimental measurements of a GEPRC EM3115 900 KV motor, 10x5x3-in propeller and HAKRC 65 A ESC were performed using an LY-10KGF thrust stand. After removing the 90% and 100% regimes, which will be explained later, 32 points remain; 20 points from 40% to 80% are used for coefficient identification. Figure 1 summarizes the traceable workflow.

2. SYSTEM AND METHODS

2.1. Tested configuration

The studied vehicle is m = 5.4 kg quadcopter. Each branch uses a GEPRC EM3115 900 KV motor [12] and a three-blade 10x5x3-in propeller shown in Figure 2. The used electronic speed controller is a HAKRC unit rated at 65 A per branch [13]. The shared source is a 6S, 10 Ah, 30 C LiPo battery. Air density is measured in each experiment and lies between 1.174÷1.175 kg/m³ at 23.2÷23.6 °C. Table 1 lists the model inputs.



Figure 2. Used 10x5x3-in propeller and GEPRC EM3115 900 KV motor

Table 1. Confirmed configuration and test environment

Item	Value
Vehicle	5.4 kg; four rotors
Motor	GEPRC EM3115, 900 KV
Propeller	10x5x3 in; three blades
ESC	HAKRC, 65 A per branch
Battery	6S LiPo; 10 Ah; 30 C;
Atmosphere	23.2÷23.6 °C; ρ=1.174÷1.175 kg m^{-3}

2.2. Analytical and identified static model

At zero advance ratio, thrust T and reaction torque M are expressed by Equations (1a) and (1b), where N is optical speed in RPM, D_p is propeller diameter, ρ is air density, C_T thrust coefficient and C_M is torque coefficient.

$$T = C_T \rho \left(\frac{N}{60}\right)^2 D_p^4 \tag{1a}$$

$$M = C_M \rho \left(\frac{N}{60}\right)^2 D_p^5 \tag{1b}$$

The geometric pitch angle θ_p, which is a function of propeller diameter D_p and propeller pitch H_p, and effective blade angle α_{ab} are defined by Equations (2a) and (2b). The corresponding analytical thrust, blade-drag and torque coefficients follow from Equations (3a) - (3c). Here A is aspect ratio, ε is the downwash correction, λ is the effective blade-area factor, ζ is the mean linear-speed factor, e is the Oswald factor, C_{fd} is the profile-drag coefficient, α_0 is the zero-lift angle and K_0 is the lift-curve slope. Recommendation for the parameter ranges for two blade ($B_p = 2$) propellers is given in [6].

$$\theta_p = tan^{-1}\left(\frac{H_p}{\pi D_p}\right) \tag{2a}$$

$$\alpha_{AB} = \varepsilon\theta_p - \alpha_0 \tag{2b}$$

$$C_{T,a} = \frac{0.25\pi^3 \lambda \zeta^2 B_p K_0 \alpha_{AB}}{\pi A + K_0} \tag{3a}$$

$$C_d = C_{fd} + \frac{\left(\frac{\pi A K_0^2}{e}\right)\alpha_{AB}^2}{(\pi A + K_0)^2} \tag{3b}$$

$$C_{M,a} = \frac{\pi^2 C_d \zeta^2 \lambda B_p^2}{8A} \tag{3c}$$

For each raw point i, the two regression ordinates are defined by Equations (4a) and (4b). The constant coefficients are then fitted through the physical origin using Equations (5a) and (5b).

$$q_{T,i} = \rho_i \left(\frac{N_i}{60}\right)^2 D_p^4 \tag{4a}$$

$$q_{M,i} = \rho_i \left(\frac{N_i}{60}\right)^2 D_p^5 \tag{4b}$$

$$\hat{C}_T = \frac{\sum q_{T,i} T_i}{\sum q_{T,i}^2} \tag{5a}$$

$$\hat{C}_M = \frac{\sum q_{M,i} M_i}{\sum q_{M,i}^2} \tag{5b}$$

With the parameters recommended from [6] for two bladed propellers: A = 5, ε = 0.85, λ = 0.75, ζ = 0.5, e = 0.83, α_0 = 0°, C_{fd} = 0.015 and K_0 = 6.11 [6]; the obtained values for our case are C_T = 0.1638 and C_M = 0.0174. The experimental fit gives C_T = 0.1506 and C_M = 0.0099. This gives significant deviations between analytical and experimental value of coefficients. Since the parameter B_p affects certain terms in equations (3a) and (3c), it is necessary to determine appropriate values for the other parameters.

Measurable parameters are changed according to case, and others analytical parameters were determined by minimizing the relative-error objective in Equation (6).

The aspect ratio A is fixed at 12.7 and it is based of used 10x5x3-in propeller; ε, λ, ζ, e and α_0 are constrained to the prescribed intervals [6]. Because λ and ζ enter only through $\lambda\zeta^2$, their individual values are not uniquely identified; the feasible pair nearest the centers of the two ranges is retained.

$$J = \left(\frac{C_{T,a}}{\widehat{C_T}} - 1\right)^2 + \left(\frac{C_{M,a}}{\widehat{C_M}} - 1\right)^2 \quad (6)$$

The solution is A = 12.7, ε = 0.918, λ = 0.812, ζ = 0.621, e = 0.80, α_0 = -0.625°, C_{fd} = 0.015 and K_0 = 6.11. It gives, C_d = 0.0363, C_{Ta} = 0.1506 and C_{Ma} = 0.0099. The experimental fit gives C_T = 0.1506 and C_M = 0.0099. Their numerical equality is a result of calibration and is not an independent validation of the geometric model.

2.3. LY-10KGF experiment and data treatment

Testing was performed on a LY-10KGF test stand Figure 3 using MET-V6 acquisition software. For the test, a single battery-ESC-motor-propeller combination was used. Between each of the four experimental measurements, the battery was fully recharged and the motor was allowed to cool to ambient temperature. The test stand specification and vendor software documentation define the measured channels. The LY-10KGF specification gives 10 kgf (98.07 N) thrust range with 0.001 kgf (0.0098 N) resolution and an error expression of 0.1% of reading plus 0.1% full scale. The corresponding torque figures are 5 Nm, 0.001 Nm resolution and 0.2% of reading plus 0.2% full scale [14,15]. Four exports contain command, optical RPM, voltage, DC current, thrust, torque, temperature and environmental data.



Figure 3. LY-10KGF test stand with GEPRC EM3115 and 10x5x3 in three blade propeller

Each of the four experimental sweeps followed a descending command sequence. The command was reduced from 100% to 10% in 10-percentage-point increments, with each level held for 5 s, and was then set to 0% to stop the system. For each sweep and command level, the samples recorded during the corresponding 5-s interval were time-averaged to obtain one representative value for each measured channel.

The original records contain ten nominal command levels, but all 90% and 100% rows are removed before calculation and plotting. These results were not used in analysis because of ESC rating and motor power limitations. At 90%, the mean branch current is 64.27 A, too close to the 65 A rating to provide a useful operating margin; at 100%, every measured branch current exceeds the rating. The retained analysis therefore contains 32 sweep-level points, corresponding to eight command levels from 10% to 80% across four sweeps. The test stand manufacturer recommends testing propulsion units producing more than 1 kgf (9.807 N) [14]. The 10÷30% points are below that level, and the 10% point has 9.7÷19.7% coefficient of variation in principal channels. The coefficient fit is restricted to 20 points from 40% to 80%. For each retained command, the arithmetic mean and sample standard deviation across four measurements are reported. The symbol ± s in the tables and figures is defined by Equation (7). s_x is standard deviation, n = 4 number of repeated measurements, x_i individual value measured during the i-th experimental run, $\bar{x}$ arithmetic mean value of all measurements.

$$s_x = \sqrt{\frac{1}{n-1}\sum(x_i - \bar{x})^2} \quad (7)$$

Agreement is evaluated with the root-mean-square error RMSE and mean absolute percentage error MAPE definitions in Equations (8a) and (8b), where y_i is the experimentally measured thrust or torque value at the i-th data point, and $\hat{y}_i$ is the corresponding thrust or torque value predicted by the model. Leave-one-sweep-out cross-validation was applied. In each of the four iterations, C_T and C_M were identified from the 40÷80% data of three sweeps and evaluated on all retained points of the remaining sweep. This procedure tests whether the identified coefficients are transferable between independent experimental runs and avoids evaluating the model using the same data employed for fitting.

$$RMSE = \sqrt{\frac{1}{n}\sum(y_i - \hat{y}_i)^2} \quad (8a)$$

$$MAPE = \frac{100}{n}\sum\left|\frac{y_i - \hat{y}_i}{y_i}\right| \quad (8b)$$

Piecewise-quadratic curves in Figure 4 are visual guides through the retained command means only. In Figure 5, both analytical curves are direct evaluations of Equations (1a) and (1b). The forward-flight map uses interpolation in measured thrust and remains entirely within the measured 40÷70% interval.

2.4. Electrical and vehicle-level calculations

The analytical motor current model uses the calibrated C_M and the interpolated optical RPM. With nominal no-load motor constant K_{V0} = 900 RPM/V, nominal no-load current I_{m0} = 2 A at nominal no-load voltage U_{m0} = 24 V and motor resistance R_m = 0.041 Ω, motor current follows Equation (9).

$$I_m = \frac{MK_{V0}U_{m0}}{9.55(U_{m0} - I_{m0}R_m)} + I_{m0} \quad (9)$$

Equations (10a) - (10d) close the motor, ESC and battery model. The ESC resistance is R_e = 0.008 Ω, battery resistance is R_b = 0.004 Ω and a conservative battery voltage of U_b = 21 V is adopted for forward-flight performance analysis. The physically admissible smaller root, $0 \leq \sigma \leq 1$, is used. K_E is back electromotive force constant, and U_{req} is the effective voltage required by the ESC-motor branch to sustain the prescribed rotational speed and torque, including the voltage drop across the ESC resistance.

$$K_E = \frac{U_{m0} - I_{m0}R_m}{K_{V0}U_{m0}} \quad (10a)$$

$$U_m = I_mR_m + K_EN \quad (10b)$$

$$U_{req} = U_m + I_mR_e \quad (10c)$$

$$U_{req} = \sigma[U_b - R_b(4\sigma I_m + I_{other})] \quad (10d)$$

Shaft power P_{shaft} and electrical-to-shaft efficiency η are calculated from synchronized channels by Equations (11a) and (11b). U is the measured DC voltage at the input of the tested ESC-motor branch.

$$P_{shaft} = \frac{2\pi NM}{60} \quad (11a)$$

$$\eta = \frac{P_{shaft}}{UI_e} \quad (11b)$$

For four equal branches and I_{other} = 1 A auxiliary consumption, total current I_b and constant-current endurance in minutes t_{fly} are given by Equations (12a) and (12b). Auxiliary consumption of 1 A is determined from datasheet of other electrical peripherals, and it was confirmed by measuring and rounding up to higher value. Battery capacity is C_b = 10 Ah and usable capacity f_{use}=0.8K_b; 80% of total battery capacity K_b, the constant-current endurance is:

$$I_b = 4I_e + I_{other} \quad (12a)$$

$$t_{fly} = \frac{60f_{use}C_b}{I_b} \quad (12b)$$

The ideal payload and force-balance tilt θ associated with a selected per-rotor thrust limit are given by Equations (13a) and (13b).

$$m_{pay} = \frac{4T_{lim}}{g} - m$$
$$m_{pay} = \frac{4T_{lim}}{g} - m \quad (13a)$$

$$\theta_{max} = arccos\left(\frac{mg}{4T_{lim}}\right) \quad (13b)$$

For conditional forward flight, required thrust per rotor is first evaluated from Equation (14).

$$T_{req}(\theta) = \frac{mg}{4cos\theta} \quad (14)$$

The conditional speed bound combines static drag balance, geometric pitch speed and the stricter minimum in Equations (15a)-(15c). V_D is the static drag-balance speed, V_p is the geometric pitch-speed bound and V_{lim} is their minimum. The projected area varies from 0.028 to 0.035 m² and the assumed drag coefficient from 2.05 to 1.80; these are unmeasured screening inputs based on bluff-body practice [16].

$$V_D = \sqrt{\frac{2mgtan\theta}{\rho S(\theta)C_D(\theta)}} \quad (15a)$$

$$V_p = \frac{NH_p}{60} \quad (15b)$$

$$V_{lim} = min(V_D, V_p) \quad (15c)$$

Finally, Equation (16) converts conditionally limited speed and endurance t_{fly} in minutes into conditional range R in kilometers.

$$R = \frac{V_{lim}t_{fly}60}{1000} \quad (16)$$

3. RESULTS

3.1. Static electrical and mechanical results

Electrical input power U·I exceed shaft power because part of the supplied power is dissipated within the ESC–motor–propeller system. The difference increases with load, primarily due to current-dependent losses and the accompanying reduction in battery voltage. The electrical-to-shaft efficiency increases from 40.2% at 10% command to the highest measured value of 65.5% at 70%, before decreasing to 63.8% at σ = 80%.

Table 2 summarizes the retained pooled measurements. From 10% to 80%, current, thrust, and torque increase monotonically with command. At the highest point the mean branch current is 44.919 A, safely below the 65 A reference line; the excluded 90% regime would leave less than 1 A margin in the highest sweep.

The corresponding current and power trends are shown in Figure 4. Electrical input power U·I exceed shaft power because part of the supplied power is dissipated within the ESC–motor–propeller system. The difference increases

with load, primarily due to current-dependent losses and the accompanying reduction in battery voltage. The electrical-to-shaft efficiency increases from 40.2% at 10% command to the highest measured value of 65.5% at 70%, before decreasing to 63.8% at σ = 80%.

Table 2. LY-10KGF measurements (mean ± sample SD)

σ [%]	N [RPM]	I [A]	T [g]	M [Nm]	η [%]
10	2246±218	0.43±0.08	88±17	0.018±0.003	40.2
20	4833±53	2.81±0.06	446±10	0.080±0.001	58.2
30	6613±49	6.70±0.09	875±15	0.147±0.001	61.8
40	7956±63	11.81±0.07	1285±12	0.213±0.002	61.5
50	9109±67	17.34±0.14	1683±21	0.276±0.003	62.6
60	10128±41	23.71±0.07	2093±9	0.345±0.002	64.1
70	11148±1	31.82±0.59	2587±35	0.425±0.008	65.5
80	12219±97	44.92±0.14	3195±9	0.526±0.003	63.8

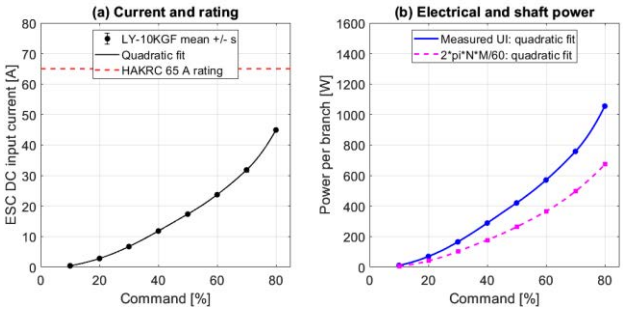


Figure 4. Retained branch current and 65 A ESC rating (a), and electrical and shaft power (b)

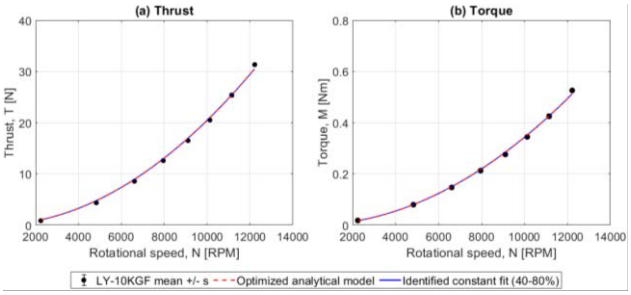


Figure 5. Static thrust (a) and torque (b) versus optical RPM

3.2. Calibrated and identified coefficients

Identification using 20 raw data points from 40% to 80% gives C_T=0.1506 and C_M=0.0099. The constrained geometric optimization produces the same values to plotting precision. **Table 3** reports the agreement metrics, and Figure 5 compares both models with pooled measurements.

Table 3. Agreement in the 40÷80% identification region

Model	C_T	C_M	T MAPE [%]	M MAPE [%]
Analytic geometry	0.1506	0.0099	2.274	2.331
Identified constant	0.1506	0.0099	2.274	2.331

The optimized geometric and identified constant curves overlap because their coefficients are numerically equal.

When evaluated against the same 20 measurements from the 40÷80% command range that were used for coefficient identification, the fitted model gives RMSE 0.5747 N for thrust and 0.00998 Nm for torque; the corresponding centered R^2 values are 0.9924 and 0.9918. Leave-one-sweep-out validation increases MAPE only slightly, from 2.274% to 2.326% for thrust and from 2.331% to 2.419% for torque. This small increase indicates that a single constant pair of C_T and C_M provides a repeatable approximation for the tested 10×5×3 propeller under static conditions within the 40÷80% command range. However, the results do not justify applying the same coefficients outside this operating range or to another propeller.

3.3. Vehicle-level analysis

Per-sweep interpolation to 1350 g per rotor gives hover at 41.65±0.32% command, 8146±91 RPM and 12.715±0.134 A per branch. Equations (12a) and (12b) give 51.86±0.54 A total and t_{fly}=9.26±0.10 min. At 70%, measured branch current is 31.82 A, total current is 128.29 A and t_{fly}=3.74 min. Mean thrust of 2587.3 g per rotor gives necessary vertical trust for steady horizontal flight at 58.55° pitch angle. Table 4 summarizes these results.

Table 4. Conditional vehicle-level results

Quantity	Conditional result
Hover	41.65%; 8146 RPM; 9.26 min
70% point	31.82 A/branch; 3.74 min
Tilt angle at σ = 70%	58.55°
Measured-current max range at θ = 12.34 °	9.363 km; 17.44 m/s; 8.95 min
Analytical-current max range θ = 12.34 °	10.338 km; 17.44 m/s; 9.88 min
Maximum conditional speed bound at σ = 70%	23.6 m/s at 58.55°

The corresponding speed and range maps are presented in Figure 6. In Figure 6a. Up to 12.344°, V_D is active; beyond the crossing, V_p is active. In Figure 6b, the blue curve uses the analytical BLDC/ESC current model with experimentally calibrated propeller loading, whereas the magenta curve directly scales the measured LY-10KGF branch current.

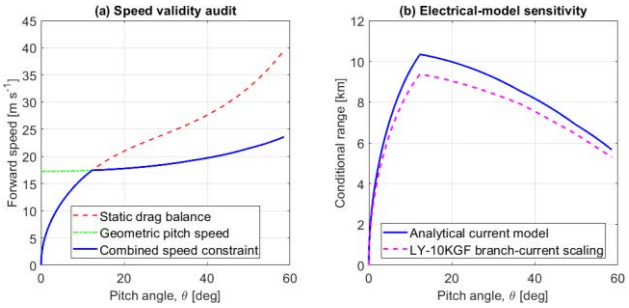


Figure 6. Conditional forward-flight analysis: speed constraints (a) and range sensitivity to the current model (b)

Both range curves peak at σ = 42.5%, θ = 12.34° and V_{lim} = 17.44 m/s. When the measured motor current is used, the estimated range is 9.363 km with t_{fly} = 8.95 min, while the analytical predicted current model gives 10.348 km of range with t_{fly} = 9.88 min, 10.42% higher. The apparent sharp decrease is a slope change at the min (V_D,V_p) constraint switch: thereafter speed grows slowly, while required thrust, current and endurance penalty continue to rise.

4. DISCUSSION

The final analytical and identified coefficients are intentionally equal. The geometric parameters were optimized against the experimental C_T and C_M, so the overlapping curves in Figure 5 demonstrate successful calibration rather than an independent theoretical prediction. The analytical formulation remains useful because it shows how the aspect ratio, blade-area factor, mean-speed factor, downwash correction and drag assumptions influence the coefficients. However, λ and ζ cannot be interpreted separately from this data set because only their product $\lambda\zeta^2$ is observable. The next step is to test other three-bladed propellers with suitable motors in order to validate or refine the selected parameters.

The exclusion of the 90% and 100% command levels is justified on both electrical and methodological grounds. The 90% mean does not exceed 65 A, but individual runs approach the rating and leave no practical current or control reserve; every 100% run exceeds the rating. Removing both regimes before analysis avoids fitting a local static model in a region dominated by component limits and heat accumulated during preceding runs. The highest retained 80% point remains within the controller rating.

The corresponding current and power trends are shown in Figure 4. The electrical input power U·I exceeds the shaft power because part of the supplied power is dissipated through losses in the ESC and motor. The absolute difference between electrical input power and shaft power increases with loading, which is consistent with the growing influence of current-dependent losses. When efficiency is evaluated separately for each experimental measurement and then averaged across the four repetitions, it rises overall from 40.2% at 10% command to the highest measured value of 65.5% at 70%, before decreasing to 63.8% at 80%.The low-command value is particularly sensitive to measurement uncertainty because both torque and input power are small. Its generally lower value reflects the greater relative contribution of no-load and weakly load-dependent losses, whereas the decrease at 80% is consistent with increasing current-dependent losses. The reported quantity is the electrical-to-shaft efficiency of the tested ESC–motor branch under static propeller loading and does not include the aerodynamic conversion efficiency of the propeller.

Directly measured current is the stronger basis for endurance because it avoids propagating any residual torque-model error through the motor equations. The 10.42% separation between the two Figure 6b curves quantify model sensitivity. The total value 128.29 A at 70% is the sum of four branches and 1 A auxiliary load; it must not be compared with the 65 A rating of one ESC.

Figure 6 remains a conditional analysis. The surface area and drag coefficients were not measured, V_p omits slip and inflow, static data do not represent oblique flow, and the calculation assumes four equally loaded rotors and constant usable battery capacity.

Future validation should combine bidirectional airspeed, attitude, RPM, voltage, current and temperature measurements with controlled battery state. Raw synchronized samples, tachometer redundancy, calibration certificates and repeated zero checks would permit a complete uncertainty budget rather than descriptive between-sweep repeatability alone.

5. CONCLUSION

Four LY-10KGF measurements provide 32 retained points from 10% to 80%. A 40-80% least-squares fit gives C_T = 0.1506 and C_M = 0.0099. Constrained calibration with A = 12.7, ε = 0.918, λ = 0.812, ζ = 0.620961, e = 0.80 and α_0 = -0.625° reproduces both coefficients. Leave-one-run-out MAPE is 2.326% for thrust and 2.419% for torque.

The results indicate that the GEPRC EM3115–HAKRC–10×5×3 combination is adequately, but not optimally, matched within the retained operating range. The 65 A ESC is adequate up to the highest retained 80% command level; however, the limited current margin at 90% and the rating exceedance at 100% indicate that it is not suitable for unrestricted operation near full command. An ESC with a higher continuous-current rating would provide greater transient-current and thermal margin and reduce the risk of controller overload. A broader continuous operating range could also be achieved by reducing the propeller load through a smaller pitch, diameter or blade number, or by selecting a motor with a lower K_V or a higher continuous-current and thermal rating. These changes must be evaluated as a complete motor–ESC–propeller system, since a higher-rated ESC or motor alone would not reduce the required current or necessarily improve efficiency.

Measured current gives hover at 8146 RPM and 41.65% command with t_{fly}=9.26 min. At 70%, t_{fly} falls to 3.741 min, while the conditional force-balance tilt reaches 58.55°. The maximum conditional range is 9.363 km when calculated from measured branch current and 10.338 km when calculated from the analytical current model. These values

support component selection and transparent design comparison, but not flight certification or validation.

Acknowledgment

This work was supported by the Ministry of Science, Technological Development and Innovation, Republic of Serbia (Contract No.451-03-34/2026-03/200325).

References

[1] ANTONIĆ, V., TRIFKOVIĆ, M., MOLOVIĆ, V., MILENKOVIĆ-BABIĆ, M.: *Small Fixed-Wing UAV Precision Aerial Drop Capability Development*, Scientific Technical Review, 74(2) (2024) pp 65-70

[2] U.S. ARMY: RQ-11B Raven Small Unmanned Aircraft System, army.mil, 4 November 2014.

[3] U.S. ARMY CENTER FOR ARMY LESSONS LEARNED: Integrating sUAS and Loitering Munitions into Company and Below, No. 26-1148, April 2026.

[4] GILL, R., D'ANDREA, R.: *Propeller thrust and drag in forward flight*, IEEE CCTA, 2017, pp. 73-79. doi:10.1109/CCTA.2017.8062443.

[5] SHI, D., DAI, X., ZHANG, X., QUAN, Q.: *A practical performance evaluation method for electric multicopters*, IEEE/ASME Transactions on Mechatronics, 22(3) (2017), pp. 1337-1348. doi:10.1109/TMECH.2017.2675913.

[6] QUAN, Q.: Introduction to Multicopter Design and Control, Springer, Singapore, 2017. doi:10.1007/978-981-10-3382-7.

[7] HWANG, M.-H., CHA, H.-R., JUNG, S.Y.: Practical endurance estimation for minimizing energy consumption of multirotor unmanned aerial vehicles, Energies, 11(9) (2018), 2221.

[8] THEYS, B., DIMITRIADIS, G., HENDRICK, P., DE SCHUTTER, J.: *Experimental and numerical study of mini-UAV propeller performance in oblique flow*, Journal of Aircraft, 54(3) (2017), pp. 1076-1084.

[9] THEYS, B., DE SCHUTTER, J.: *Forward flight tests of a quadcopter UAV with various spherical body diameters*, International Journal of Micro Air Vehicles, 12 (2020), pp. 1-8.

[10] YE, J., WANG, J., SONG, T., et al.: *Propulsion optimization of a quadcopter in forward state*, Aerospace Science and Technology, 113 (2021), 106703.

[11] POLLET, F., DELBECQ, S., BUDINGER, M., MOSCHETTA, J.-M.: *Design optimization of multirotor drones in forward flight*, ICAS 2021, HAL hal-03832135.

[12] GEPRC: EM3115 900KV Motor - Official Product Specification , https://geprc.com/product/geprc-em3115-900kv-motor/, accessed 12 July 2026.

[13] HAKRC: 65A ESC - Official Product Specification, https://www.hakrc.com/HAKRC-4234-6S-65A-Airplane-Monobloc-ESC.html, accessed 12 July 2026.

[14] WING FLYING TECHNOLOGY: LY-10KGF Motor and Propeller Test System - Specification, 2021.

[15] WING FLYING TECHNOLOGY: MET-V5 Software User Manual, 2021.

[16] HOERNER, S.F.: Fluid-Dynamic Drag, published by the author, Midland Park, NJ, 1965.